Program Digest, 2019 IEEE International Ultrasonics Symposium (IUS)
Glasgow, Scotland, October 6-9, 2019

Asymmetric energy coupling through acoustoelectric effect using graphene on lithium niobite surface acoustic wave delay line in GHz Range

Christopher Carmichael
Electrical & Computer Engineering Department
University of Central Florida
Orlando, FL. USA
carmichael.chris@knights.ucf.edu

Donald C. Malocha
Pegasense, LLC
Winter Springs Fl., USA
dcmalocha@cfl.rr.com
+*Electrical & Computer Engineering Department*
University of Central Florida
Orlando, FL. USA

Arthur Weeks
Electrical & Computer Engineering Department
University of Central Florida
Orlando, FL. USA
arthur.weeks@ucf.edu

***Abstract*—Technology advances provide new processes for the fabrication and application of novel materials to acoustoelectric devices. An important advancement would be the ability to produce practical integrated SAW AE amplifiers. Notably for practical applications, devices will need to be capable of operating with a continuous drift field applied rather than the most often-cited timed pulse approach and be cheaply manufacturable. With ultra-high mobility materials, such as graphene, power reduction can be achieved with the asymmetrical AE effect under a constant applied drift field.**

This paper will present a new embodiment of a graphene-based AE structure on LiNbO3. The first part of the paper will discuss the theory behind the SAW AE amplifier, including the critical film parameters for the maximum gain. The second part will present a new design and results from recent research efforts to conform graphene to have more ideal thin film parameters for the AE effect

Keywords— surface acoustic wave, acoustoelectric, graphene

I. Introduction (*Heading 1*)

The foundations for Surface Acoustic Wave (SAW) Acousto Electric (AE) theory date back all the way to the 1960's, where doped semiconductors were suspended with an air gap above the propagating surface of a SAW carrying piezoelectric substrate [1][2][3][4][5]. While early devices were able to demonstrate the asymmetric amplifying affect, they were subject to many problems making manufacturing, reproducibility, and practical applications impossible. More recent research in this area has eliminated the airgap method in favor of thin films or direct bonded mediums to create manufacturing processes with greater reproducibility [6][7][8][9]. The basic embodiment is shown in Fig. 1. The ability to produce a practical integrated SAW AE amplifier in filters and other devices would provide new opportunities for SAW RF filters and oscillators. However, to date no practical devices have been shown which operate with net amplification in continuous wave (CW) operation, both of which are requirements for practical applications of these devices. The ideal material parameters to achieve a practical integrated SAW AE amplifier will be discussed in this paper.

Graphene is of particular interest as it has many unique properties which are highly beneficial for current embodiments of these devices. It can be created and applied at the wafer level reproducibly as a monolayer, which decreases the physical load when applied directly to a propagating surface of a piezoelectric substrate, and as a monocrystalline solid it has ultra-high carrier mobility reported in excess of 200,000 $\frac{cm^2}{V*s}$ in a free-standing film [10]. Graphene is limited, however, by its simplicity; as a monolayer it is difficult to alter the material parameters such

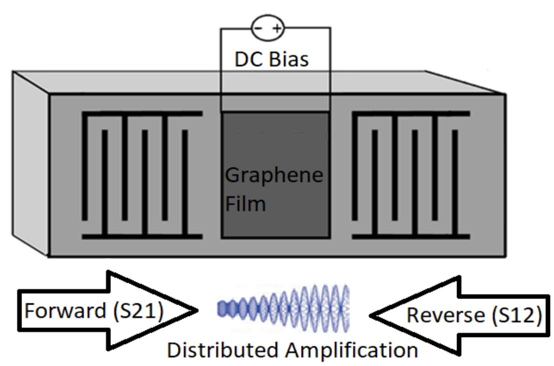

Fig. 1. Basic SAW delay line device embodiment. Delay line consists of two interdigital bidirectional transducers with a patterned ultra-thin graphene film in the free-surface delay line path. A DC bias voltage is applied to the graphene film creating an applied electric field parallel to the propagation direction [11].

This work was sponsored by the Defense Advanced Research Project Agency (DARPA) Signal Processing at RF (SPAR) program under contract number HR0011-17-C-0017. The views, opinions, and/or findings contained in this article are those of the authors and should not be interpreted as representing the official views or policies of the Department of Defense or the U.S. Government.

as carrier concentrations and sheet conductivity without breaking the monocrystalline structure and greatly reducing the sought-after carrier mobility [ref needed here].

This paper provides results of a new device embodiment which uses multi-stage distributed AE elements. The approach uses metal-oxide gates and the field-effect to modulate the conductivity of graphene used in the interaction layer of a SAW AE amplifier.

II. Backround and Design Considerations

A. AE Effect

When the traveling AE potential created by a SAW propagates through a thin film interactive layer, free charge carriers in the film are gathered and pulled along the interaction length with this traveling potential at the speed of the SAW.

When an external drift field is added to the thin film interaction layer in the SAW propagation direction, it is possible to increase or decrease the SAW potential through the AE affect. If the external drift field causes carriers in the interaction layer to move in the same direction as the SAW induced movement of the carriers, the SAW potential will increase and there is gain as shown in Fig. 1 [11].
The net current in the thin film layer is

$$J_{drift} = J_{SAW} + J_{Ext} = qn(V_{SAW} - V_c)\ , \qquad (1)$$

where *Vsaw* is the SAW velocity (determined by substrate), *Vc* is the free carrier charge velocity where $V_c = \mu \cdot \boldsymbol{\xi}_{Ext}$ (where μ is the carrier mobility, $\boldsymbol{\xi}_{Ext}$ is the applied external DC field and n is the carrier concentration *(#/cm²)*. High film mobility is desirable to reduce the external field required for a given velocity. The fraction of the SAW induced displacement current to the total current is [11]

$$\chi = \frac{J_{SAW}}{J_{drift}} = \frac{V_{SAW}}{(V_{SAW} - V_C)} \qquad (2)$$

With an applied external field to the film, the velocity and attenuation constant equations become [11]

$$v \approx v_0 \left[1 + \frac{k^2}{2} \left(\frac{\left(\frac{R_S}{Z_{SAW}} \cdot \chi^{-1} \right)^2}{1 + \left(\frac{R_S}{Z_{SAW}} \cdot \chi^{-1} \right)^2} \right) \right] \qquad (4)$$

$$\alpha = \left(\frac{2\pi}{\lambda} \right) \left(\frac{k^2}{2} \right) \left(\frac{\left(\frac{R_S}{Z_{SAW}} \cdot \chi^{-1} \right)}{1 + \left(\frac{R_S}{Z_{SAW}} \cdot \chi^{-1} \right)^2} \right) \qquad (5)$$

where $Z_{SAW} = (\varepsilon \cdot V_{SAW})^{-1}$, and k^2 is coupling coefficient. The SAW impedance is obtained from the dielectric constant and velocity, which represents stored charge in the capacitance traveling at SAW velocity.

When the carrier drift velocity due to the external field is greater than the SAW velocity, the term χ in (2) becomes negative, and the propagation constant, from (5), becomes negative which indicates device is now operating in AE gain mode.

B. Substrate and thin film parameters

The magnitude of the gain achieved per wavelength while in AE gain mode is dominated by the SAW material coupling coefficient (k^2), the carrier drift velocity, and the ratio of the impedance of the interaction film and the SAW material ($\frac{R_S}{Z_{SAW}}$). Substrates like Lithium Niobite (LN) are chosen due to their relatively high coupling coefficients (${k^2}_{YZ_{LN}} \cong 4.8\%,\ {k^2}_{128_{LN}} \cong 5.4\%,$). Their respective SAW impedances are: $Z_{YZ_{LN}} = .65M\Omega, and\ Z_{128_{LN}} = .47\ M\Omega.$ These are relatively high impedances and not typical for high mobility thin film materials. The maximum gain occurs when $R_s \sim Z_{SAW}$. The AE SAW structure presented here as a potential approach of modulating the carrier concentration for control of the thin film resistivity. Ideal thin film parameters require relatively high mobility in order to achieve realizable CW gain mode operation and relatively high resistivity such that $R_s \sim Z_{SAW}$ to maximize the coupling of energy in equation (5). This indicates that the thin film should simultaneously have low carrier concentration and high mobility while providing minimal elastic losses to the SAW; all challenging parameters to obtain in a thin film.

III. Graphene Film Impedance Modulation Results

Graphene is an extremely attractive new material for AE gain devices due to its ultra-high mobility, reported as high as 200,000 $(cm^2)/(V \cdot s)$ [10], its ability to be easily deposited and defined using photolithography, and the minimal elastic losses that a mono-layer can incur in a SAW device. Previous work has shown these devices in CW gain mode operation with up to 3 dB of asymmetric operation measured by the ratio of forward to reverse gain on 128_LN [12]. While graphene can easily show the possibility for CW gain mode operation due to its ultra-high mobility, the magnitude of the effect is greatly reduced due to the relatively low impedance of graphene when compared to the SAW impedance.

A new embodiment was created to modulate the carrier concentration in a graphene film using a field effect device design shown in Fig. 2. Test devices were made using Trivial Transfer Graphene™ (TTG) from ACS Material. The

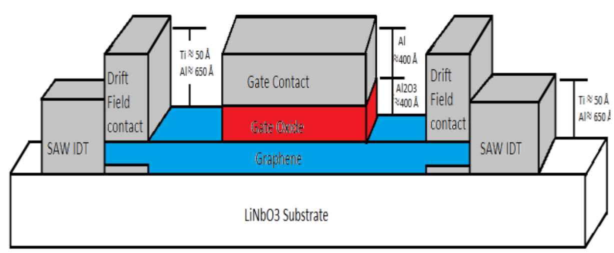

Fig. 2 Cross section of SAW AE amplifier layout with metal-oxide gate structures for conductivity modulation of graphene interaction layer.

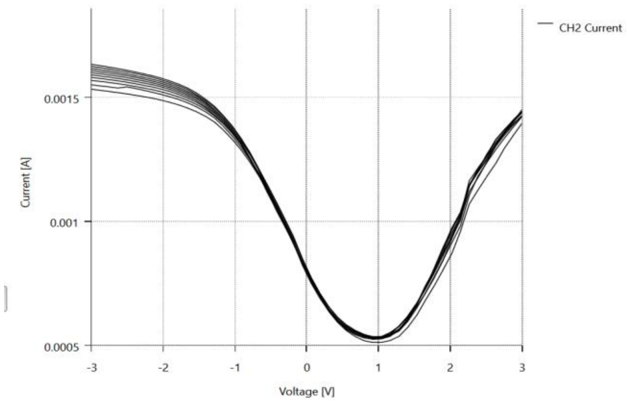

Fig. 3: 10 consecutive sweeps of current measured through ultra-thin film graphene with 2V applied at drift field contacts, while sweeping voltage applied at gate contact from -3V to 3V.

film is a predominantly single layer graphene which is created through chemical vapor deposition. TTG consists of single crystal graphene sandwiched between a water-soluble polymer and a protective polymethyl methacrylate (PMMA) protective coating. Detail of the material properties is available from ACS Material on the WEB. The graphene is transferred to the substrate by first soaking the TTG sheet in de-ionized water, to remove the water-soluble polymer and expose the graphene, then lifting the sheet into place on the target substrate, drying it thoroughly, and removing the protective PMMA coating with a soak in solvent. The graphene film is then patterned to be contained in the SAW propagation path through photolithography and oxygen plasma etch, with a length of 0.864 mm and a width of 0.33 mm. Surface acoustic wave generating interdigital transducers and graphene drift field contacts are then created through photolithography and electron beam deposition. Finally, aluminum oxide is deposited through electron beam physical vaper deposition over the AE film with a thickness of 40 nm, covering 0.635 mm of the film's length, and a 40 nm aluminum gate structure is deposited on top as seen in Fig. 2.

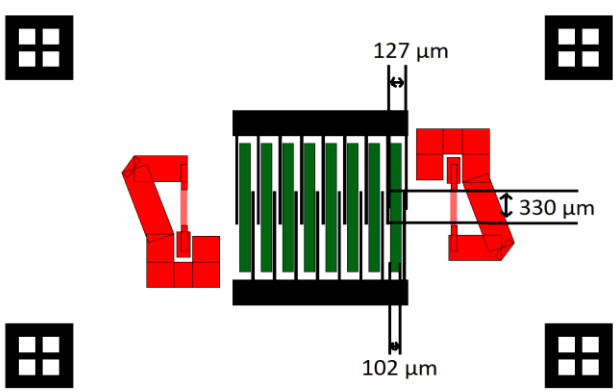

Fig. 4: Acoustic beam width was 30 wavelengths, with split electrodes, having a 1/4 wavelength period of 2.75 µm; yielding a fundamental operating frequency of approximately 311MHz AE gain structure has 8 sequential stages each with graphene measuring 127 µm in length and 330 µm in width. The gate oxide structures were 102 µm of the total length in each stage

Fig. 5: Custom vacuum system for measuring bonded multi-segment AE devices. System has 4 coaxial feed throughs, 2 are used for RF 2-port measurements and the other two are used for DC biasing of the graphene

I-V curves are measured using a Keysight B2901A by applying a potential on this gate structure from -3 V to 3 V and measuring the current through the graphene film while a constant 2 V is applied across the length of the film through the drift field contacts. As shown in Fig. 3, the impedance of the film can be modulated with the field effect through this gate/oxide structure (change in current). With a measured impedance value of approximately 975 **Ω**/☐ with 0V applied at the gate and a peak impedance of approximately 1500 **Ω**/☐ with 1 V applied at the gate we see an increase of approximately 53.9% (0 V compared 1 V) with relatively low voltages applied to the gate. Additional research into oxide materials and deposition techniques to achieve a compatible thin film oxide with higher breakdown voltages is required for this simple embodiment to become more effective.

In order to reach the field strengths required to achieve gain mode operation through the AE affect prescribed in section 2, a multi segment design was used, shown in Fig. 4, which reduces the voltage requirement for reaching the desired field strength by shortening the length of the graphene film; additional segments are then added in series to increase the total interaction length.

IV. AE Effect with Film Impedance Modulation

Devices were fabricated on YZ-LN wafers, *k^2*= 4.6% which provides good AE coupling, and *V_saw* = 3488 m/s.

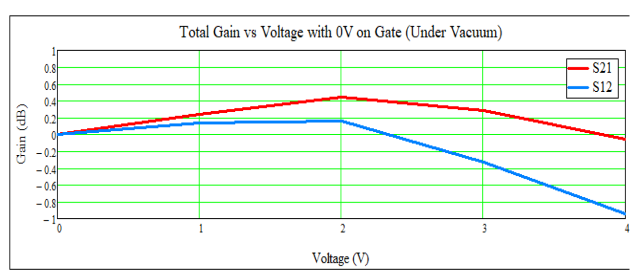

Fig. 6: Vacuum measurements of SAW peak S21 and S12 values at 933MHz with 0V applied at gate, normalized to 0 V applied at AE drift contacts. With varying DC fields applied to each graphene AE drift contact segments in the propagation path of the delay line.

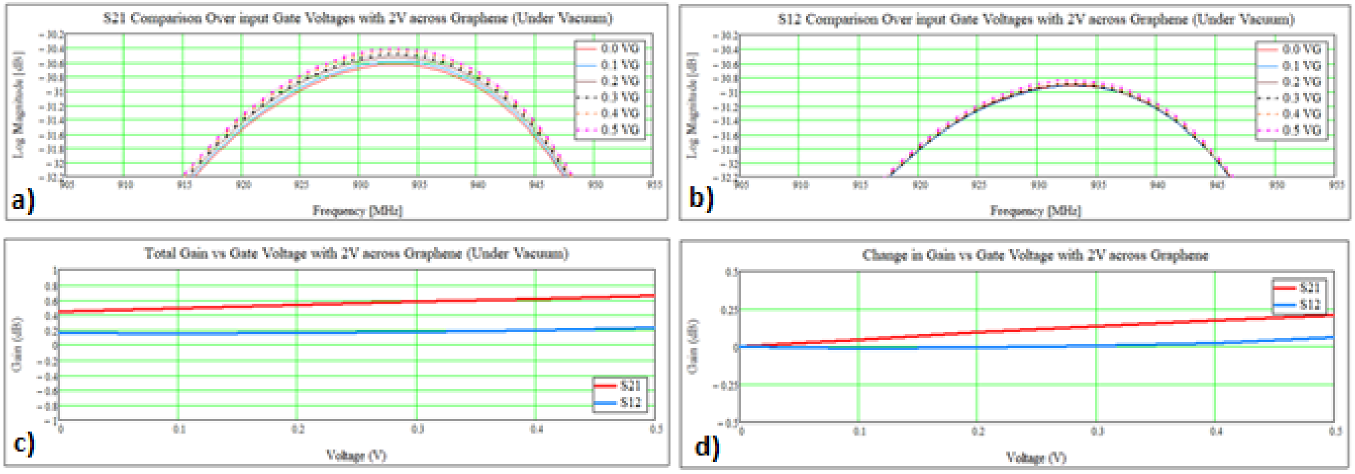

Fig. 7: Narrowband SAW frequency responses at center frequency of 933MHz with 2 V DC electric field applied to ultrathin film graphene in propagation path of delay line and varying DC Voltages applied to metal-oxide gate. (a) Forward SAW frequency response with varying DC voltages applied to metal-oxide gate with 2 V electric field applied to thin film graphene, (b) Reverse SAW frequency response with varying DC voltages applied to metal-oxide gate with 2 V electric field applied to thin film graphene, (c) Plot of total forward and reverse SAW peak values verses applied DC voltage on Metal-oxide gate while 2 V electric field is applied to thin film graphene (d) Plot of total forward and reverse SAW peak values verses applied DC voltage on Metal-oxide gate while 2 V electric field is applied to thin film graphene normalized to 0 V applied to gate-oxide.

The acoustic beam width was 30 wavelengths, with split electrodes, having a 1/4 wavelength period of 2.75 µm; yielding a fundamental operating frequency of approximately 311MHz. The AE gain stage for these devices included 8 sequential stages each with graphene measuring 127 µm in length and 330 µm in width. The gate oxide structures were 102 µm of the total length in each stage. The following data was obtained at the third harmonic of 933 MHz

Devices were diced and bonded out in to gold-plated die packages and a custom fixture and vacuum chamber were made for measurements, shown in Fig. 5. With 0 V applied to the gate the SAW frequency responses were measured with varying DC fields applied to ultrathin film graphene segments in the propagation path of the delay line. SAW peak S21 and S12 values at 933MHz were then recorded and are shown in Fig. 6. The peak forward energy gained from the AE graphene stages was recorded at approximately 0.4 dB with 2 V applied across each graphene segment.

With 2 V applied across each stage of the amplifier the gate voltages were then swept from 0 V to 0.5 V as shown in Fig. 7. In the forward direction an increase in the normalized signal strength is observed. Measurements show S21 $\approx$ 0.65 dB with 0.5 V applied to the gate. These measurements show an increase of asymmetric energy coupling through the AE effect of approximately 0.2 dB forward and 0.4 dB reverse. The measurements demonstrate the asymmetry changes predicted from equation (5) whenever the ratio of impedances of the substrate and the AE interaction material is altered.

Acknowledgment

This work was sponsored by the Defense Advanced Research Project Agency (DARPA) Signal Processing at RF(SPAR) program under contract number HR0011-17-C-0017. The authors gratefully acknowledge support by Rockwell Collins, Inc. under the DARPA SPAR program contract.

References

[1] A. R. Hutson, and D. L. White. "Elastic wave propagation in piezoelectric semiconductors." Journal of Applied Physics 33, no. 1: 40- 47, 1962.

[2] D. L. White, "Amplification of ultrasonic waves in piezoelectric semiconductors." Journal of Applied Physics 33.8: 2547-2554, 1962.

[3] K. A. Ingebrigtsen, "Elab Report TE-94." Norwegian Institute of Technology, Trondheim, Norway, 1967.

[4] J. H. Collins, K. M. Lakin, C. F. Quate, and H. J. Shaw, “Amplification of acoustic surface waves with adjacent semi-conductor and piezoelectric crystals.” Appl. Phys. Lett. 13, 314-316, 1968.

[5] K. M. Lakin, H. J. Shaw, “Surface wave delay line amplifiers.” IEEE Trans. Microwave Theory Tech., vol. MTT-17, No. 11 912-920, 1969.

[6] Y. Chen, H. Zhang, H. Zhang, Z. Feng, H. Zhao, C. Sun, S. Zheng, W. Pang, and D. Zhang, “Acoustically induced current in graphene by aluminum nitride transducers.” *Appl. Phys. Lett.* 108 033107, 2016.

[7] V. Miseikis, J. E. Cunningham, K. Saeed, R. O’Rorke, and A. G. Davies, “Acoustically induced current flow in graphene.” *Appl. Phys. Lett.*100 133105, 2012.

[8] L. Bandhu, L. M. Lawton, and G. R. Nash, “Macroscopic acoustoelectric charge transport in graphene.” *Appl. Phys. Lett.* 103, 133101, 2013.

[9] P. V. Santos, T. Schumann, M. H. Oliveira, Jr., J. M. J. Lopes, and H. Riechert, “Acousto-electric transport in epitaxial monolayer graphene on SiC.” *Appl. Phys. Lett.* 102 221907, 2013.

[10] K. I. Bolotin, K. J. Sikes, Z. Jiang, M. Klima, G. Fudenberg, J. Hone, P. Kim, H.L Stormer, “Ultrahigh electron mobility in suspended graphene.” Solid State Comm. 146, 351-355, 2008.

[11] D. C. Malocha, C. Carmichael, M. S. Smith and A. Weeks, "Thin Film Acoustoelectric GHz SAW Amplifier Design," *2018 IEEE International Ultrasonics Symposium (IUS)*, Kobe, 2018, pp. 1-4

[12] C. P. Carmichael, M. S. Smith, A. R. Weeks, D. C. Malocha, "Experimental Investigation of Surface Acoustic Wave Acoustoelectric Effect using a Graphene Film on Lithium Niobate", IEEE Transactions on Ultrasonics Ferroelectrics and Frequency Control.